PHYSICAL REVIEW B **78**, 060404(R) (2008)

Ultrafast magnetostriction and phonon-mediated stress in a photoexcited ferromagnet

C. v. Korff Schmising,[1] A. Harpoeth,[1] N. Zhavoronkov,[1] Z. Ansari,[1] C. Aku-Leh,[1] M. Woerner,[1,*] T. Elsaesser,[1] M. Bargheer,[2] M. Schmidbauer,[3] I. Vrejoiu,[4] D. Hesse,[4] and M. Alexe[4]

[1]*Max-Born-Institut für Nichtlineare Optik und Kurzzeitspektroskopie, Max-Born-Strasse 2a, 12489 Berlin, Germany*

[2]*Institut für Physik und Astronomie, Universität Potsdam, Karl-Liebknecht-Strasse 24-25, 14476 Potsdam, Germany*

[3]*Leibniz-Institut für Kristallzüchtung, Max-Born-Strasse 2, 12489 Berlin, Germany*

[4]*Max-Planck-Institut für Mikrostrukturphysik, Weinberg 2, 06120 Halle, Germany*

(Received 17 July 2008; published 18 August 2008)

Femtosecond excitation of $SrRuO_3$ nanolayers in a $SrRuO_3/SrTiO_3$ superlattice quenches their ferromagnetism, resulting in magnetostriction. The buildup of mechanical stress is observed in real time by mapping lattice motions via ultrafast x-ray diffraction. A rise time of 500 fs is found for a wide range of excitation wavelengths. In the ferromagnetic phase, phonon-mediated (σ_{ph}) and magnetostrictive stress (σ_M) components display similar strengths but opposite signs. The amplitude of σ_M follows the temperature dependent magnetization $M^2(T)$ whereas the strength of σ_{ph} is determined by the amount of deposited energy.

DOI: 10.1103/PhysRevB.78.060404 PACS number(s): 75.80.+q, 61.05.C−, 78.47.−p

Changes in electronic and/or spin correlations in solids are associated with atomic rearrangements on multiple length and time scales. In addition to transitions between metallic, insulating, or magnetic phases,[1] magnetostriction, the change in a solid's dimension upon changing its magnetization,[2,3] represents a prototype phenomenon of this type. In ferromagnets, magnetostriction plays a key role for the reorientation of magnetic domains in an external field and for the so-called invar effect, the temperature independent volume of a larger class of ferromagnets below their Curie temperature.[4,5] In such systems, the positive thermal expansion due to anharmonic phonon-phonon interactions is compensated by a negative magnetostrictive contribution. Beyond its fundamental relevance, magnetostriction finds increasing application in sensors and actuators, including nanolayered and/or nanostructured devices. So far, however, the nonequilibrium dynamics of magnetostriction is not fully understood. In particular, the time scale on which magnetostrictive stress builds up after changing ferromagnetic correlations is not known.

Transition metal oxides with a perovskite crystal structure feature a rich variety of electronic correlations closely linked to the geometry of the crystal lattice. A prominent example is $SrRuO_3$ (SRO) which crystallizes in a slightly distorted cubic unit cell, exhibits metallic conductivity, and becomes ferromagnetic below the Curie temperature of $T_C \approx 160$ K.[6] SRO represents an itinerant ferromagnet in which the strong hybridization of Ru $4d$ and O $2p$ orbitals leads to delocalized ferromagnetically ordered electrons.[6–10] This picture is supported by a number of measurements of the magnetic moment that is somewhat smaller than for localized electrons (e.g., Ref. 11). The invar effect of bulk SRO measured in x-ray and neutron-scattering studies[12–14] points to a pronounced interplay between structural degrees of freedom and electronic properties.[6,9] Nanolayers of SRO display an extraordinarily anisotropic saturation magnetization as a function of both the direction of an applied magnetic field and the tetragonal distortion of the crystal, i.e., at $T=0$ the crystal exhibits a huge magnetovolume effect.[15,16] Recent femtosecond magneto-optical Kerr measurements[17] suggest that optical excitation reduces the macroscopic magnetization of SRO on a subpicosecond time scale. The related structural dynamics of the material, i.e., the change in atomic positions in the lattice induced by the generated magnetostrictive stress has, however, remained unknown.

Addressing transient magnetostriction calls for measuring the transient atomic positions in the material on the subpicosecond time scale of atomic motions. A separation of such elementary structure changes from strain propagation occurring with the velocity of sound requires samples of small thickness. Ultrafast x-ray diffraction from superlattices (SLs) with a tailored sequence of layer pairs and SL phonon modes as specific probes allows for mapping structure changes with a 100 fs temporal and a subpicometer spatial resolution.[18,19] In this Rapid Communication, we present an ultrafast time resolved x-ray structure analysis to directly measure the buildup of optically induced uniaxial stress in the ferromagnetic nanolayers of a $SrTiO_3$ (STO)/SRO SL. The photoinduced stress excites coherent fully reversible oscillations of the SL with a 3 ps period. The phase and amplitude of such oscillations provide direct insight into the buildup of transient stress and its magnetostrictive component. A rise time of 500 fs is found for a wide range of excitation wavelengths. In the ferromagnetic phase, phonon-mediated and magnetostrictive stress components display similar strengths, the latter decreasing with increasing sample temperature T. In the paramagnetic phase (sample temperature $T>160$ K), the phonon-mediated stress dominates and shows an amplitude determined by the amount of deposited excess energy.

The sample studied here was fabricated by pulsed-laser deposition[20] and consists of ten double layers of STO/SRO on a 50 nm thick SRO buffer layer grown epitaxially on a STO substrate. The equilibrium structure of the sample is derived from static x-ray reflectivity measurements in combination with dynamic x-ray diffraction theory.[19,21] Figure 1(a) shows a high-resolution reciprocal space map around the asymmetric Bragg reflection (1 0 3) of the STO substrate. It plots the intensity of the STO substrate and SL Bragg peaks on a logarithmic scale as a function of the in- and out-of-plane reciprocal-lattice vectors q_a and q_c, respectively. It unambiguously demonstrates pseudomorphic growth with the

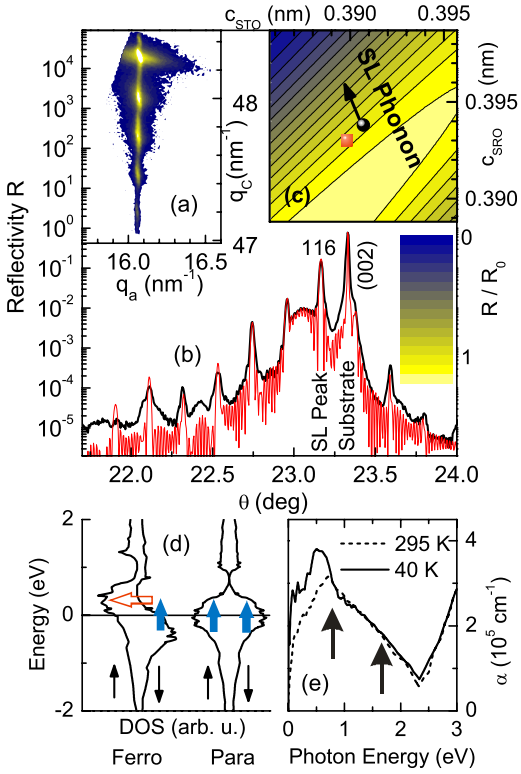

FIG. 1. (Color online) (a) Measured reciprocal space map of the SL showing pseudomorphic growth of the sample. (b) Thick line: measured x-ray reflectivity of the SL as a function of the diffraction angle θ. Thin line: calculated reflectivity of the sample using dynamical x-ray diffraction theory. (c) Contour plot of the calculated intensity of the (0 0 116) SL Bragg peak as a function of the lattice parameters c_{STO} and c_{SRO}. The circle and square indicate the initial structure at 300 and 22 K, respectively. The arrow shows the motion of the SL phonon along these coordinates. (d) Density of states (DOS) of majority ($\downarrow$) and minority ($\uparrow$) spins in the ferromagnetic and paramagnetic phases according to Ref. 9. Vertical solid arrows: spin-conserving optical transitions; horizontal open arrow: magnon involved in spin-flipping indirect transitions. (e) Frequency dependent absorption coefficient $\alpha(\omega)$ of $SrRuO_3$ calculated from the experimental data of Ref. 26 (arrows: pump frequencies).

in-plane lattice parameter a of the SL structure being dictated by the STO substrate. Figure 1(b) is a $\theta/2\theta$ scan around the (0 0 2) STO Bragg reflection at 23.3°. The scan shows the reflectivity of the SL sample on a logarithmic scale as a function of the diffracting angle θ and reveals strong SL Bragg peaks. The SL period d_{SL} gives rise to equidistant maxima (00ℓ) at Bragg angles θ corresponding to multiples $G=\ell g_{SL}$ of the reciprocal SL vector $g_{SL}=2\pi/d_{SL}$. The structural parameters averaged over the equilibrium structure of the SL are $a_{STO}=c_{STO}=0.391$ nm, $c_{SRO}=0.394$ nm, $d_{STO}=15.24$ nm, and $d_{SRO}=7.48$ nm with $d_{SL}=d_{STO}+d_{SRO}$. We find an excellent agreement between measurement and simulation.

In the femtosecond experiments, the sample is excited by a 50 fs pump pulse which interacts exclusively with the SRO layers, and the resulting lattice response is probed by a delayed ultrashort hard x-ray pulse (Cu $K\alpha$, photon energy of 8.05 keV, $\lambda=0.154$ nm), generated in a laser-driven x-ray plasma source.[22] Changes in the intensity diffracted on the (0 0 116) SL Bragg peak are measured as a function of pump-probe delay. For the experiments presented here, we placed the sample in a cryostat allowing for sample temperatures between $T=20$ and 300 K. The x-ray probe beam was focused onto the sample with a multilayer x-ray mirror (Montel optic), resulting in a spot size of approximately $d=150$ μm.[23] Pump-probe measurements were performed in a broad range of excitation wavelengths between 800 nm and 2.2 μm.

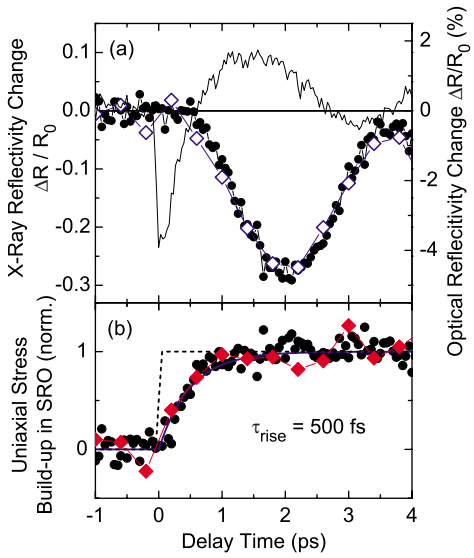

FIG. 2. (Color online) (a) Transient change in the x-ray reflectivity $\Delta R/R_0$ after ultrafast optical excitation at $\lambda_{ex}=800$ nm (circles) and $\lambda_{ex}=2.2$ μm (open diamonds) with the same pump fluence of the SRO layers in the STO/SRO superlattice ($T=300$ K). Thin line: (800 nm) pump / (800 nm) probe experiments serve for an exact determination of delay zero. (b) Time evolution of the uniaxial stress in the SRO layers derived from the data in (a) ($T=300$ K, solid circles) and in Fig. 3(c) ($T=20$ K, solid diamonds).

In Fig. 2(a), we present the transient change in x-ray intensity $\Delta R/R_0$ reflected from the sample at $T=300$ K after excitation at $\lambda_{ex}=800$ nm (circles) and $\lambda_{ex}=2.2$ μm (open diamonds). The pump fluence of approximately 6.5 mJ/cm^2 results in the excitation of several tens of percent of free electrons. The transients show a delayed rise and oscillations with a period of 3 ps. Zero time delay is measured with an accuracy of ± 100 fs using an all-optical reflectivity measurement in the same setup [thin line in Fig. 2(a)]. Data taken with different pump wavelengths and fluences show the same time behavior. The amplitude of the signal is determined by the absorbed pump fluence, independent of the pump wavelength.

Data for a wide range of lattice temperature are summarized in Fig. 3. We present both (a) the optical reflectivity change probed at $\lambda_{pr}=2.2$ μm and (c) the transient change in the x-ray reflectivity (symbols) measured after excitation at $\lambda_{ex}=2.2$ μm with identical pump fluence. For all temperatures, the optical pump-probe data [Fig. 3(a)] show a coherent artifact (peak) around delay zero and a fast decay ($\tau_{fast}\approx 250$ fs), followed by a steplike component persisting for

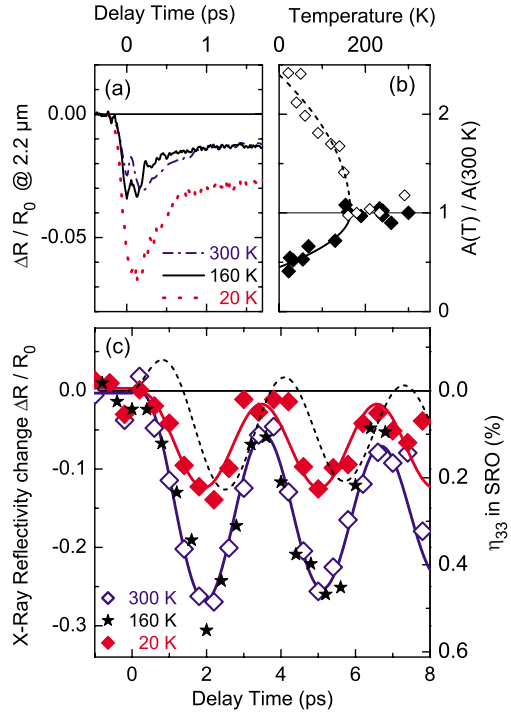

FIG. 3. (Color online) (a) Optical reflectivity change at $\lambda_{pr}=2.2$ μm and (c) transient change in the x-ray reflectivity (symbols) measured with excitation at $\lambda_{ex}=2.2$ μm at various lattice temperatures. Solid lines: fits with $\tau_{rise}=\tau_{mag}=500$ fs. Dashed line: simulation with $\tau_{mag}=0$. (b) Temperature dependence of the amplitude $A(T)$ of the optical $\Delta R/R_0$ (open diamonds) and the SL phonon oscillation (solid diamonds) normalized to the respective value at $T=300$ K. In the ferromagnetic phase ($T<T_C=160$ K), the amplitude of the all-optical transients is enhanced, while the SL phonon amplitude is reduced due to the magnetic contractive stress contribution. Both amplitudes follow approximately the temperature dependent magnetization squared $M^2(T)$ (dashed and solid lines).

hundreds of picoseconds, similar to recent ellipticity data.[17] Time resolved x-ray intensity changes in the (0 0 116) SL reflection for different temperatures [Fig. 3(c): 300 K (open diamonds), 160 K (stars), and 20 K (solid diamonds)] display an identical time evolution, i.e., initial delay, oscillation period, and phase. In both the all-optical and x-ray transients, the essential signature varying with the lattice temperature is the maximum signal amplitude which is plotted as open diamonds (all optical) and solid diamonds (x ray) in Fig. 3(b) normalized to their respective values at room temperature. In the ferromagnetic phase ($T<T_C=160$ K), the amplitude of the all-optical transients is enhanced, while the SL oscillation amplitude in the x-ray transients drops significantly toward $T=0$. Both amplitudes follow the measured[14] temperature dependent magnetization squared $M^2(T)$ [lines in Fig. 3(b)].

We now discuss the physical mechanisms underlying the oscillatory fully reversible changes in x-ray reflectivity. The femtosecond pump pulse induces an electronic excitation of the SRO layers which generates a mechanical stress of the lattice via the coupling of the electronic system to lattice degrees of freedom. In our excitation scheme of the SL, this uniaxial stress is spatially periodic and drives a spatially periodic strain wave. Such structural changes are mapped into the x-ray diffraction pattern, in general changing both the angular position and the intensity of the SL Bragg peaks. The periodic reflectivity changes and the unchanged angular positions found in our experiments give evidence of a periodic modulation in time of the layer thicknesses d_{SRO} and d_{STO} at a constant SL period d_{SL}, corresponding to coherent SL phonon oscillations.[18,19] Their period of 3 ps is determined by d_{SL} and the velocity of sound. The thickness modulation is equivalent to a geometry change along the c axes of the SRO and STO lattices which are parallel to the SL stack axis.

Figure 1(c) shows the calculated reflectivity of the (0 0 116) SL Bragg peak as a function of the c-axis parameters c_{STO} and c_{SRO} normalized to the equilibrium values at $T=300$ K (circle). Driving SL oscillations corresponds to the arrow with an expansion of the SRO layers d_{SRO} and concomitant compression of the STO layers d_{STO} at constant d_{SL}.[21] The slope of the arrow is determined by the respective thicknesses of the layers. The equidistance of the contour lines in this area shows that the reflectivity-strain mapping is linear and remains unchanged for different sample temperatures [square in Fig. 1(c) for $T=20$ K]. From the maximum amplitude of the reflectivity changes plotted in Fig. 2(a) and the contour plot of Fig. 1(c), one derives a maximal strain in the SRO layers of $\eta_{33}^{SRO}=c_{SRO}(2\ \text{ps})/c_{SRO}(t<0)-1=5\times10^{-3}$.

The data in Figs. 2(a) and 3(c) demonstrate a delayed onset of the SL oscillations. We derive the driving force $F(t)$, i.e., photoinduced uniaxial stress, from the differential equation $d^2\eta_{33}^{SRO}/dt^2-\omega_0^2\eta_{33}^{SRO}=F(t)$ with the SL oscillation frequency ω_0. $F(t)$ [Fig. 2(b)] shows a noninstantaneous rise. The rise time $\tau_{rise}=500$ fs is independent of excitation wavelength and sample temperature, as is evident from a comparison of the $T=20$ K (diamonds) and $T=300$ K (circles) data. The noninstantaneous rise demonstrates that direct stress generation by electronic excitation[18] plays a minor role here. Instead, the generation of a nonequilibrium phonon population by electron cooling and—in the ferromagnetic phase at $T<160$ K—magnetostriction are the main sources of stress. In the all-optical experiments [Fig. 3(a)], the ultrafast decrease in reflectivity and the subsequent subpicosecond recovery reflect the ultrafast thermalization and the cooling of photoexcited electrons, as is known from extensive studies of carrier dynamics in metals.[24] Our data show that (i) such processes occur in SRO within the first 500 fs and (ii) this time scale—and thus the electron-phonon coupling strength—is very similar for all lattice temperatures between 20 and 300 K, i.e., in the ferromagnetic and paramagnetic phases. Such electron cooling times are shorter than the rise time of stress in the SL. The buildup of magnetostriction will be addressed below.

In the paramagnetic phase ($T\geq160$ K), magnetostriction is absent. The rise time of stress represents the buildup of the nonequilibrium phonon population driving the SL oscillations with a temperature independent amplitude [solid symbols in Fig. 3(b)] exclusively determined by the amount of deposited energy. In the ferromagnetic phase ($T<160$ K), both phonon generated and magnetostrictive stress components occur. Their superposition results in a pronounced change in the strain amplitude with temperature. This amplitude change mimics the temperature dependent magnetiza-

tion $M^2(T)$ [solid line in Fig. 3(b)]. The amplitude reduction is caused by the contractive magnetic contribution to the stress which originates from the strong magnetovolume effect present in bulk[12,14] and even more pronounced in nanolayered SRO.[15,16] At $T=20$ K, the magnetostriction reaches a very high value of approximately $\eta_{33}^{\mathrm{SRO}}=-2.5\times10^{-3}$, in quantitative agreement with the expected magnitude for SRO nanolayers grown on STO substrate.[15,16]

It is important to note that the buildup kinetics of stress [Fig. 2(b)] and—thus—the phase of the SL oscillations [symbols in Fig. 3(c)] is identical in the paramagnetic and ferromagnetic phases. We conclude that the rise time of the magnetostrictive stress component is very similar to that of the nonequilibrium phonon component, i.e., 200 fs$<\tau_{\mathrm{mag}}<$700 fs. In particular, a sub-100 fs rise of magnetostriction can be ruled out as is evident from a simulation of SL oscillations driven by an instantaneous magnetostrictive and a delayed phonon-mediated stress [dashed line in Fig. 3(c)].

The amplitude of our optical pump-probe data [Fig. 3(a)] shows the same temperature dependence [Fig. 3(b)] as ultrafast demagnetization experiments on $SrRuO_3$.[17] Thus, the demagnetization and the concomitant buildup of magnetostrictive stress occur during the subpicosecond cooling period of the electron gas, i.e., the decay of the transients in Fig. 3(a). Spin-orbit interaction in SRO allows for spin-flipping intraband scattering processes,[9] e.g., absorption of a photon (solid vertical arrow) followed by emission of a magnon [open horizontal arrow in Fig. 1(d)]. In the ferromagnetic phase, the combined density of states between the majority ($\downarrow$) and minority ($\uparrow$) spin bands derived from band-structure calculations[9] shows a pronounced peak at an energy of $\hbar\omega\approx0.6$ eV. This energy corresponds exactly to our excitation wavelength $\lambda_{\mathrm{ex}}=2.2$ μm [cf. Fig. 1(e)] where the photoinduced magnetostriction is found to be strongest.[25]

In conclusion, we have identified different mechanisms of ultrafast stress generation in the itinerant ferromagnet SRO. Measuring photoinduced structural dynamics in real-time by ultrafast x-ray diffraction, we provide direct evidence for a subpicosecond magnetostriction in nanolayered SRO. The amplitude of the magnetostrictive component of transient stress decreases with increasing temperature, mimicking the temperature dependent $M^2(T)$. The magnetostrictive stress compensates a major fraction of the crystal expansion driven by nonequilibrium phonons.

We gratefully acknowledge the financial support by the Deutsche Forschungsgemeinschaft (Grant No. SPP1134).

*woerner@mbi-berlin.de

[1] A. Cavalleri, C. Toth, C. W. Siders, J. A. Squier, F. Raksi, P. Forget, and J. C. Kieffer, Phys. Rev. Lett. **87**, 237401 (2001).
[2] L. W. McKeehan and P. P. Cioffi, Phys. Rev. **28**, 146 (1926).
[3] S. C. Masmanidis, H. X. Tang, E. B. Myers, M. Li, K. De Greve, G. Vermeulen, W. V. Roy, and M. L. Roukes, Phys. Rev. Lett. **95**, 187206 (2005).
[4] R. J. Weiss, Proc. Phys. Soc. London **82**, 281 (1963).
[5] J. L. Robertson, G. E. Ice, C. J. Sparks, X. Jiang, P. Zschack, F. Bley, S. Lefebvre, and M. Bessiere, Phys. Rev. Lett. **82**, 2911 (1999).
[6] I. I. Mazin and D. J. Singh, Phys. Rev. B **56**, 2556 (1997).
[7] J. S. Lee, Y. S. Lee, T. W. Noh, S. Nakatsuji, H. Fukazawa, R. S. Perry, Y. Maeno, Y. Yoshida, S. I. Ikeda, J. Yu, and C. B. Eom, Phys. Rev. B **70**, 085103 (2004).
[8] K. Fujioka, J. Okamoto, T. Mizokawa, A. Fujimori, I. Hase, M. Abbate, H. J. Lin, C. T. Chen, Y. Takeda, and M. Takano, Phys. Rev. B **56**, 6380 (1997).
[9] D. J. Singh, J. Appl. Phys. **79**, 4818 (1996).
[10] P. B. Allen, H. Berger, O. Chauvet, L. Forro, T. Jarlborg, A. Junod, B. Revaz, and G. Santi, Phys. Rev. B **53**, 4393 (1996).
[11] J. M. Longo, P. M. Raccah, and J. B. Goodenou, J. Appl. Phys. **39**, 1327 (1968).
[12] T. Kiyama, K. Yoshimura, K. Kosuge, Y. Ikeda, and Y. Bando, Phys. Rev. B **54**, R756 (1996).
[13] B. Dabrowski, M. Avdeev, O. Chmaissem, S. Kolesnik, P. W. Klamut, M. Maxwell, and J. D. Jorgensen, Phys. Rev. B **71**, 104411 (2005).
[14] S. N. Bushmeleva, V. Y. Pomjakushin, E. V. Pomjakushina, D. V. Sheptyakov, and A. M. Balagurov, J. Magn. Magn. Mater. **305**, 491 (2006).
[15] O. Gan, R. A. Rao, C. B. Eom, J. L. Garrett, and M. Lee, Appl. Phys. Lett. **72**, 978 (1998).
[16] K. Terai, T. Ohnishi, M. Lippmaa, H. Koinuma, and M. Kawasaki, Jpn. J. Appl. Phys., Part 2 **43**, L227 (2004).
[17] T. Ogasawara, K. Ohgushi, Y. Tomioka, K. S. Takahashi, H. Okamoto, M. Kawasaki, and Y. Tokura, Phys. Rev. Lett. **94**, 087202 (2005).
[18] M. Bargheer, N. Zhavoronkov, Y. Gritsai, J. C. Woo, D. S. Kim, M. Woerner, and T. Elsaesser, Science **306**, 1771 (2004).
[19] C. v. Korff Schmising, M. Bargheer, M. Kiel, N. Zhavoronkov, M. Woerner, T. Elsaesser, I. Vrejoiu, D. Hesse, and M. Alexe, Phys. Rev. Lett. **98**, 257601 (2007).
[20] I. Vrejoiu, G. Le Rhun, L. Pintilie, D. Hesse, M. Alexe, and U. Gösele, Adv. Mater. (Weinheim, Ger.) **18**, 1657 (2006).
[21] C. von Korff Schmising, M. Bargheer, M. Kiel, N. Zhavoronkov, M. Woerner, T. Elsaesser, I. Vrejoiu, D. Hesse, and M. Alexe, Appl. Phys. B: Lasers Opt. **88**, 1 (2007).
[22] N. Zhavoronkov, Y. Gritsai, M. Bargheer, M. Woerner, T. Elsaesser, F. Zamponi, I. Uschmann, and E. Förster, Opt. Lett. **30**, 1737 (2005).
[23] M. Bargheer, N. Zhavoronkov, R. Bruch, H. Legall, H. Stiel, M. Woerner, and T. Elsaesser, Appl. Phys. B: Lasers Opt. **80**, 715 (2005).
[24] S. D. Brorson, J. G. Fujimoto, and E. P. Ippen, Phys. Rev. Lett. **59**, 1962 (1987).
[25] Additional measurements with an identical pump fluence at $\lambda_{\mathrm{ex}}=800$ nm show that the magnetostrictive contribution to the stress in the ferromagnetic phase is three times smaller than after excitation at $\lambda_{\mathrm{ex}}=2.2$ μm.
[26] P. Kostic, Y. Okada, N. C. Collins, Z. Schlesinger, J. W. Reiner, L. Klein, A. Kapitulnik, T. H. Geballe, and M. R. Beasley, Phys. Rev. Lett. **81**, 2498 (1998).